ELSEVIER

Available online at www.sciencedirect.com

ScienceDirect

New Astronomy 00 (2015) 1–8

New Astronomy

High resolution reconstruction of solar prominence observed by New Vacuum Solar Telescope

Yong-yaun Xiang[a,b,*], Zhong Liu[a], Zhen-yu Jin[a]

[a] *Yunnan Observatories, Chinese Academy of Sciences, Kunming, China, 650011*
[b] *University of Chinese Academy of Sciences, Beijing, China,100049*

Abstract

High resolution observation of solar prominence contributes to the studying of their fine structures and physical characteristics. We successfully implement the high resolution reconstruction of the solar prominence using speckle imaging methods. The data reconstruction is based on the observations at Fuxian Solar Observatory of Yunnan Astronomical Observatories by the New Vacuum Solar Telescope (NVST). In the absence of adaptive optics contribution, each step of the speckle reconstruction especially the data alignment is carefully processed, the highly effective alignment of full field and subfield leading to a superior reconstruction. The reconstruction indicates that under normal seeing conditions, the high resolution observation of the prominence by ground-based telescope is totally feasible.

Keywords:
Methods: solar image reconstruction; Techniques: speckle masking; Sun: prominence

1. Introduction

Solar prominences are thread-like clouds consisting of relatively cool, dense magnetized plasma suspended in the hot tenuous corona (Tandberg-Hanssen, 1995). They are one of the most striking features in the solar atmosphere. The study of prominence is very important for understanding its formation and equilibrium, even its connection and relationship with other activities. In recent years, high resolution observation found there are many small scales such as upflows, downflows and vortices inside the prominences (Berger et al., 2008, 2010; Yan et al., 2015). The deep understanding of these complex motions needs more high resolution observational data to address.

As we all know that the high resolution observation of ground-based telescope mainly rely on adaptive optics (AO) and image reconstruction techniques. The AO can compensate wavefront distortion in real time to improve the imaging quality, while the image reconstruction recovers the object high resolution information by post processing. In modern high resolution observation, the two techniques are often used together. Among numerous reconstruction techniques, speckle imaging is one of the most effective techniques. The most popular methods in speckle imaging are known as Labeyrie (Labeyrie, 1970) method, Knox-Thompson (Knox and Thompson, 1974) method and speckle masking (Weigelt, 1977; Weigelt and Wirnitzer, 1983; Lohmann et al., 1983).

*Corresponding author
Email address: binghe065@ynao.ac.cn (Yong-yaun Xiang)

Within the last 30 years a great deal of solar activity such as pore, sunspot has been successfully observed using speckle imaging method or combined with AO (von der Lühe, 1994; Denker, 1998; Denker et al., 2005; Mikurda and von der Lühe, 2006). However, prominence hardly appears in those successful observations. The main difficult of the high resolution observation of prominence is the poor AO tracking at the solar limb, and the low image signal-to-noise ratio (SNR) which seriously reduce the accuracy of the image reconstruction.

We all know that applying the speckle imaging method for solar high resolution reconstruction, the image motion of each sequence should be well corrected if it is significantly greater than the "seeing". For most of the solar scene, the residual image motion is small and negligible (Denker et al., 2005) after the correcting by AO or a simple correlation tracker (CT) system (Cao et al., 2010). However, in the prominence observation, the AO cannot work well or even cannot "lock" the target when the telescope pointing at the solar limb, the image motion correction also called frame registration or full field alignment should finish by post processing.

In this paper, we use the speckle masking method to reconstruct solar prominences observed in NVST (Liu et al., 2014). We improved the cross correlation method (Smithson and Tarbell, 1977; von der Lühe, 1983) to make sure our prominence data well aligned. Other steps such as anisoplanatism treatment, amplitude and phase recovery are carefully handled. Base on careful treatment, we successfully implement the high resolution reconstructing of the prominence and other solar limb activities.

2. Data observation

All prominence data presented in this paper are observed in the NVST chromosphere channel with band Hα (6563 Å). The NVST is a vacuum solar telescope with clear aperture 985 mm, it has come into operation since year 2012. One of the most important equipment in NVST is multi-channel high resolution imaging system, which has several channels to observe solar photosphere and chromosphere. All observation channels are connected by an optical splitter, so they can sync observe and record images. The data recording in chromosphere channel using a PCO2000 CCD with full image size 4008 × 2672 pixels and image scale 0.082″. In our observation, the central 2048 × 2048 pixels are chosen to match the view of field 168″ × 168″, and image size is binned to 1024 × 1024 pixels by the CCD settings for shortening the acquisition time and improving image SNR. Thus the image scale is 0.164″, and the collection rate is 8.3 frames per second. During the prominence observation, the AO system is closed, and the exposure time was set 20 *ms* to increase photon number. Although the exposure time seems to be a little long than the atmospheric coherence time (typically a few milliseconds). But in the actual observations, the exposure time can be several tens of milliseconds (Tyler et al., 1994).

3. Prominence reconstruction

3.1. Solar speckle imaging

The theoretical basis of speckle imaging is the atmospheric turbulence theory and linear imaging theory. Consider a sequence of images with exposure time shorter than the atmospheric correlation time, and their field does not exceed the size of the isoplanatic region. The Fourier spectrum $I(q)$ of each image $i(x)$ can be described as

$$I(q) = O(q) \cdot H(q) \ , \tag{1}$$

q denotes two-dimensional frequency variable, $O(q)$ is the Fourier spectrum of undisturbed object intensity distribution, $H(q)$ is the instantaneous optical transfer function (OTF).

From this sequence images, object Fourier amplitude and phase is respectively estimated by calculating their averaged power spectrum and average bispectrum. The averaged power spectrum can be described as

$$\langle |I(q)|^2 \rangle = |O(q)|^2 \cdot \langle |H(q)|^2 \rangle \, , \tag{2}$$

where the angular brackets $\langle ... \rangle$ denotes ensemble averages, where $\langle |H(q)|^2 \rangle$ is called speckle transfer function (STF), which can be obtain by computing Korff (1973) model if r_0 is known. The r_0 can estimate by the spectral ratio method (von der Lühe, 1984). The sequence images average bispectrum can be described as

$$\langle B(p,q) \rangle = \langle I(p) \cdot I(q) \cdot I^*(p+q) \rangle \, , \tag{3}$$

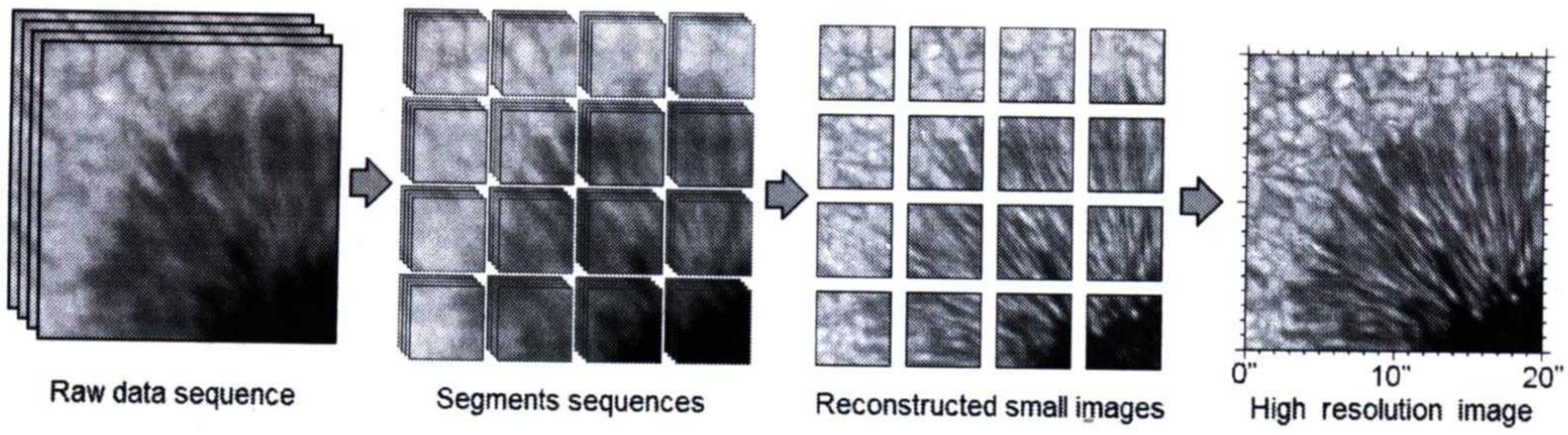

Figure 1. The high resolution reconstruction process of a solar scene. The raw data sequence is segmented into many small sequences, each small sequence is reconstructed independently, finally all small reconstructed images mosaic into a full field image.

where, $*$ denotes conjugate operator, p is two-dimensional frequency variable like q. Based on the assumption of the bispectrum transfer function is a real function (Lohmann et al., 1983), the object phase ϕ_O and bispectrum phase ϕ_B are connected by the following formula

$$\phi_O(p+q) = \phi_O(p) + \phi_O(q) - \phi_B(p,q) \ . \tag{4}$$

The object amplitude can be obtain by the de-convolution of the average power spectrum with STF, and object phase can be obtained according to Eq.4 by a recursion algorithm (Pehlemann and von der Lühe, 1989).

Basic process of high resolution reconstruction of solar image has been summarized by many researchers (see von der Lühe (1993); Mikurda and von der Lühe (2006)). In a normal process, the raw date are firstly pre-processed by flat-fielding, artifact removal and image motion correction if it is needed. After that, the full field images have to be divide into many overlapping sub images because the speckle imaging method is only valid in the isoplanatic region, then each sub images were multiplied by an apodization window to restrain the edge effect. After amplitude and phase reconstruction of each sub image sequence, an inverse Fourier transform of the recombination of the amplitude and phase can obtain the reconstructed subfield. Then all reconstructed subfield images are reassembled to a full field. A simple diagram of high resolution reconstruction process of a solar scene is shown in Figure 1.

3.2. Key point for prominence

3.2.1. Alignment method

The basic process of the prominence reconstruction is almost the same as the other solar scene such as sunspot, granulation. However, some process such as image motion correction is necessary and is not easy to implement. As the AO cannot work well at the solar limb, the full field alignment should done by post processing, in which the cross correlation method is widely used. The cross correlation function $C(\delta_x)$ of an object image $i(x)$ and reference image $k(x)$ can describe as

$$C(\delta_x) = i(x) \otimes k(x) \, . \tag{5}$$

$\otimes$ denotes correlation operator. δ_x denotes the spatial translation of x. In normal circumstances, the position vector x_M of the correlation function maximum represents the true displacement $\triangle x$ between the object and reference images. Shifting the object image with opposite x_M can make it well aligned with reference. However, the "correlation error" which represents the inconformity of x_M and $\triangle x$ often occurs in prominence alignment. This is due to the low SNR and mutation edge intensity distribution of the prominence (typical examples can see in Figure 2). Thus, an improved cross correlation method needs to propose to ensure a good aligning. We modified the input function $i(x)$ and $k(x)$ in Eq.5 by a devisable filter which was created according to their spatial frequency information to avoid "correlation error" occurring. In this case, the modified cross correlation function can express as

$$C^{'}(\delta_x) = i(x)^{'} \otimes k(x)^{'} \, . \tag{6}$$

What have been improved in the improved cross correlation?

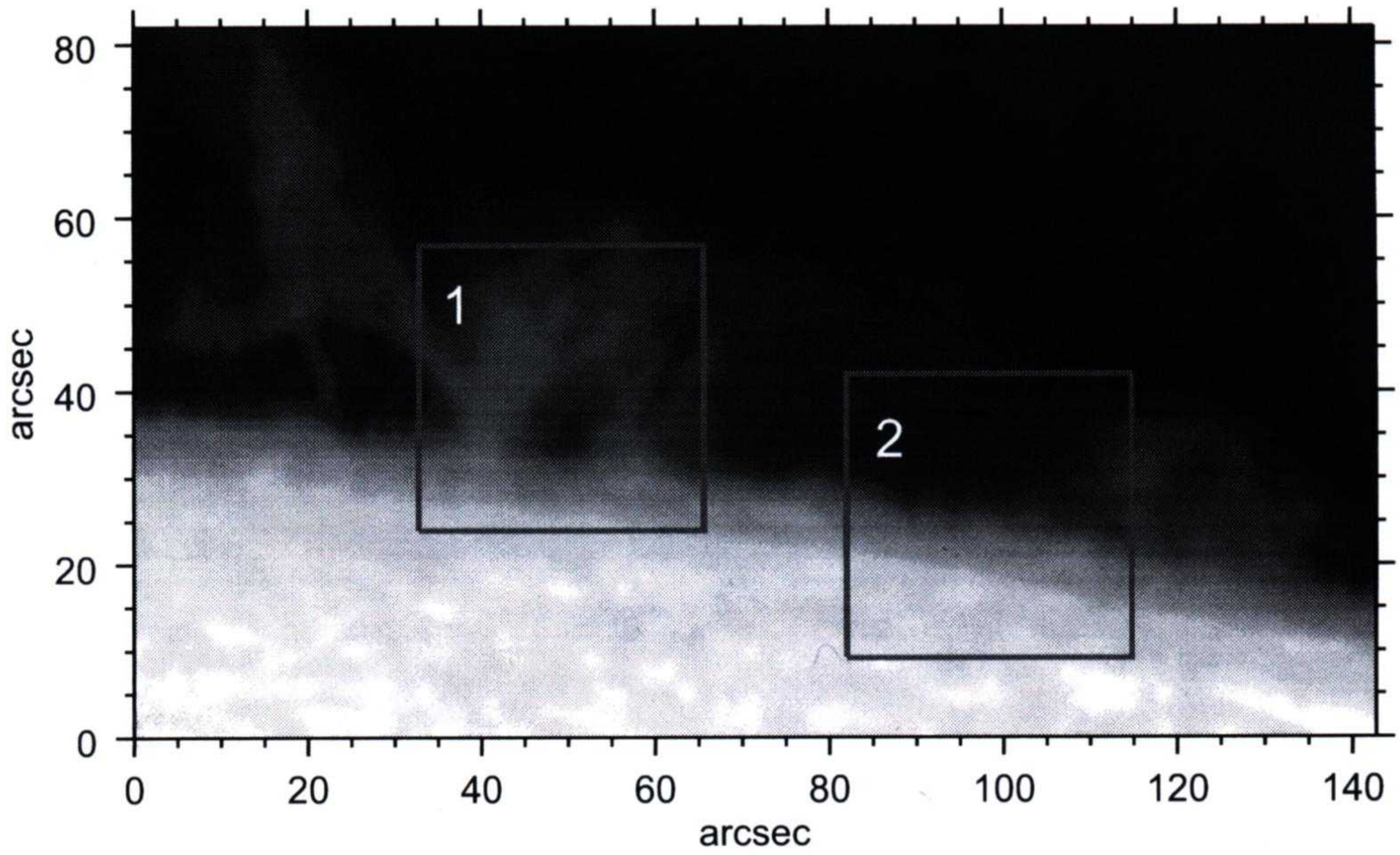

Figure 2. One short exposure image of a prominence observed on 2014 May 24, two small regions both with size 31″ × 31″ are marked with red box 1 and 2, these two regions reflected the structural characteristics of the prominence.

3.2.2. Full field alignment

The aim of full field alignment is to remove the frame-to-frame image motion ~~of full field~~. The image motion comes from the telescope tracking error and near surface turbulence. It may be large enough to be corrected, especially for the open dome telescope. Taken the NVST for example, the maximal full field image motion can reach more than 10 arcsec above four levels of wind (Liu et al., 2011). The method proposed in Section 3.2.1 was used to align full field images. The filter here used was a band-pass filter, which can well remove the low-frequency components. With the modified cross correlation method the full field images were well aligned (see instances in Movie0).

3.2.3. Subfield alignment

Subfield alignment is a step to adjust the small shacking of image due to anisoplanatism. Like the full field alignment, same alignment method was also adapted for subfield. In order to compare the results of the improved correlation method and the conventional correlation method, the distribution of correlation maximum was analysed. A histogram of the maximum distribution with this two cross correlation method for region 1 and region 2 was shown in Figure 3. For region 1, the mean vector is 0.2899″ in X direction and −1.5286″ in Y direction for conventional cross correlation, while the result is −0.0001″ and −0.0647″ for modified cross correlation. For region 2, the result is 1.2876″ and −0.4183″ for conventional cross correlation, while is 0.0127″ and −0.0792″ for modified cross correlation. Form the test we can see, the central of vector distribution with conventional cross correlation are far from the origin of coordinate system which supposed to be the center of the true vector distribution, while the result with modified cross correlation are basically equal to the origin of coordinate. The test result clearly told us that, for both the region 1 and region 2, the "correlation error" has occurred with the conventional cross correlation method, and implies a very bad subfield alignment. In contrast, the result with modified cross correlation is more credible.

To illustrate the influence of alignment with those two cross correlation methods on the reconstruction, we reconstructed the sequence with the subfield aligned using those two methods. Figure 4(a) is the result with the normal cross correlation, Figure 4(b) is the result with the modified method. To further evaluate the result, we improved a criterion proposed by Deng et al. (2015) to evaluate the similarity of the averaged image and the reconstructed image. In the

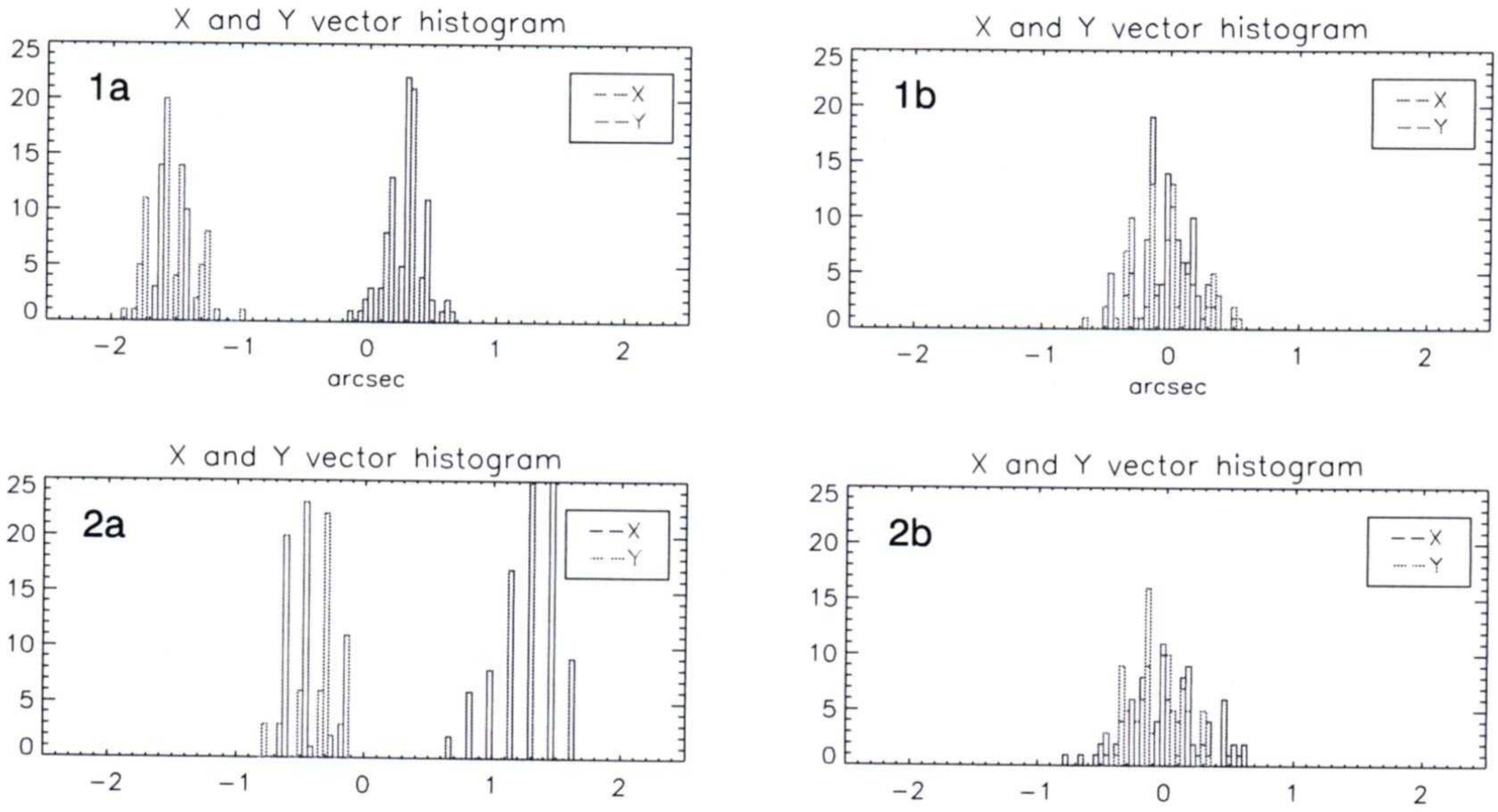

Figure 3. Histogram of 100 maximum position vectors obtained from 100 short exposure images with two different cross correlation methods for region 1 and region 2. The sub figures '*a' are the histograms of X direction (blue line) vector and Y direction (red line) vector with conventional cross correlation. The sub figures '*b' are the results with modified correlation. The x-axis are normalized to arcsec, the bin of the histogram plot here are set 0.04″.

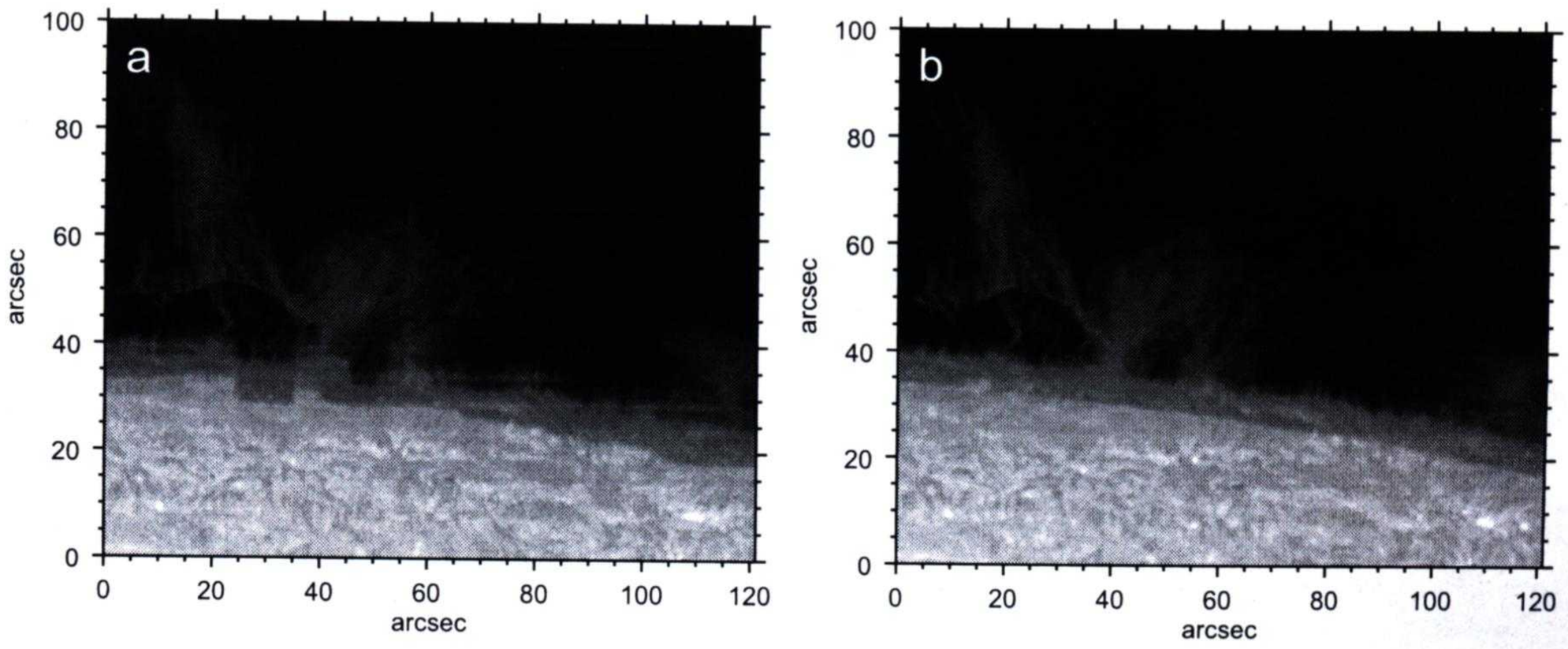

Figure 4. The reconstruction results with subfield aligned using conventional cross correlation method and modified method.

(a), (b) ?

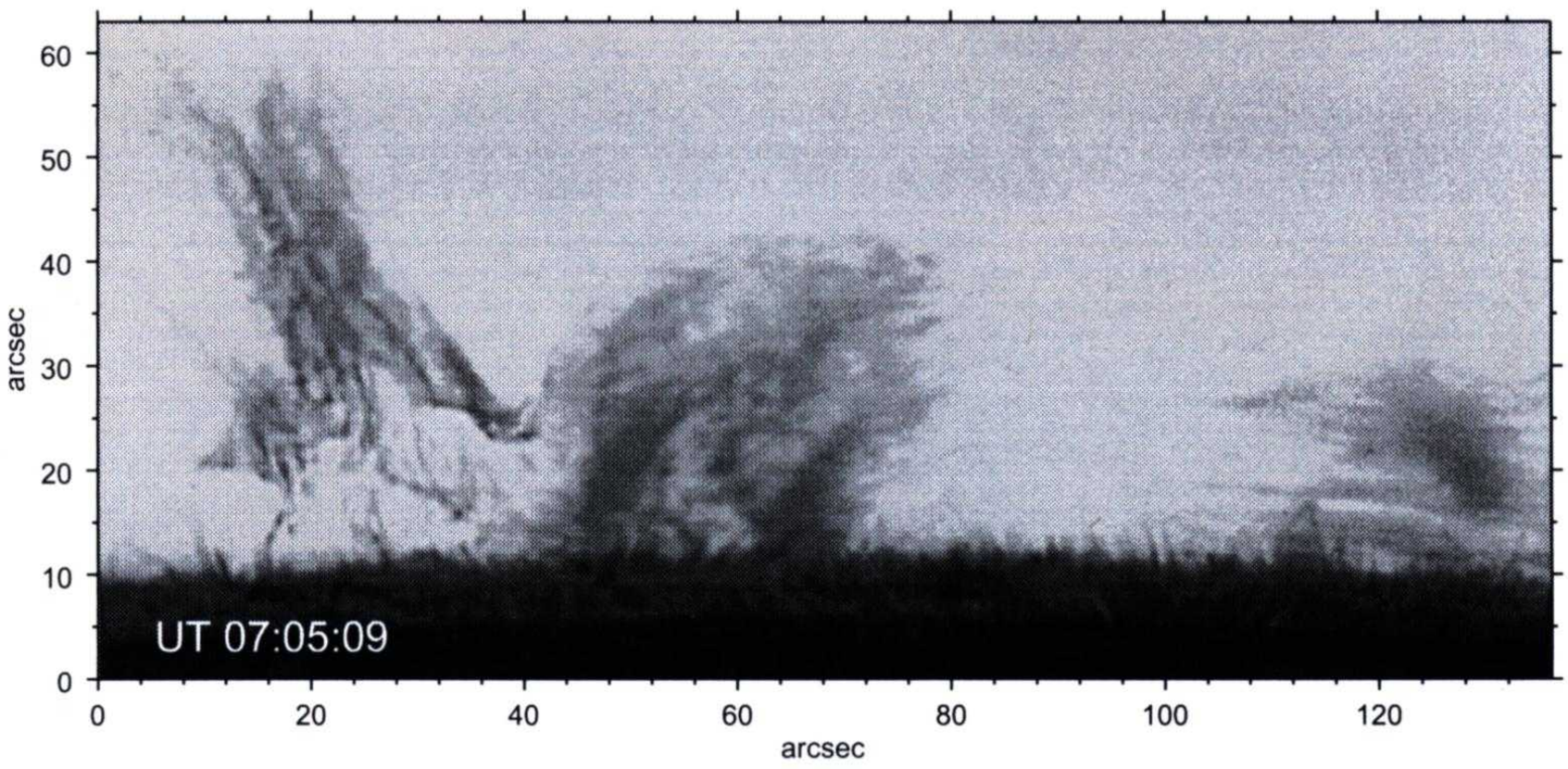

Figure 5. One high resolution reconstruction result of a prominence observed on 2014 May 24. The field of view is 136″ × 63″.

improved criterion, the fine structure of the averaged image and reconstructed image were extracted by a band-pass filter then the correlation coefficient was calculated. The coefficients are 0.31 for Figure 4(a) and 0.84 for Figure 4(b). This indicates that the alignment error of subfield seriously affect the authenticity of reconstruction results.

4. Results and discussion

In our reconstruction, each sequence using 100 frames short exposure images, and the time cadence is 12 seconds. In the data segmentation, the subfield size is 16 arcsec, and the apodization ratio of window is set 45%. During the subfield amplitude and phase restoration, the r_0 was obtained by the spectral ratio method, and the speckle transfer function (STF) was calculated by the Korff (1973) model. Each process included preprocessing, alignment, and speckle reconstruction has been carefully handled.

Two days observation data are represented here to illustrate the effectively speckle masking method for prominence reconstruction. Data one was a typical prominence observed on 2014 May 24 from 06:38 to 09:03 UT, data two was a flare ring observed on 2015 March 20 from 05:41 to 07:49 UT. A total of 695 and 635 high resolution reconstruction images was respectively obtained (See Movie1, Movie2). Each image series were then aligned with a sub-pixel alignment algorithm (Feng et al., 2012; Yang et al., 2015) for next studying, part of the reconstruction result is respectively shown in Figure 5 and Figure 6. From the high resolution reconstruction result of data one, we clearly see some high resolution structures like spine, bubble even ubiquitous counter-streaming mass flows. A detailed analysis of this prominence can see the paper of Shen et al. (2015).

The accurate alignment is very important for ensuring the accuracy of the prominences reconstruction whether it is a full field alignment or a subfield alignment. The method proposed in Section 3.2.1 is effective to avoid the "correlation error" occurring when using the cross correlation algorithm to align the prominence data. It should be noted that, the filter in this method is the key point, it should be carefully designed according to the characteristics of the target. In addition to the alignment, the r_0 estimating and de-convolution are also very important in the prominence reconstruction. In our experiments, sometimes, the recovery of the Fourier amplitude seems not the best. This may be due to the mismatch of the r_0 or some other unknown factors that affect the STF. However, this has not analyzed in this paper. We will study this in our next work.

We have successfully implemented the speckle imaging method for the high resolution reconstruction of solar prominence in NVST. Much care should be taken for preparatory work before reconstructing, especially the image alignment. An improved cross correlation method was proposed for full field alignment and subfield alignment. With

the highly effective alignment, not only the prominence but also other solar limb activity can well be reconstructed. We believe that the high resolution reconstruction result will aid the basic scientific understanding of prominences and other solar limb activities.

Acknowledgements

The authors thank NVST team, especially the observation group colleagues for they excellent observation. This work is partially supported by the National Natural Science Foundation of China (Grant Nos. 11203077, 11203074, 11473064).

References

Berger, T. E., Shine, R. A., Slater, G. L., Tarbell, T. D., Title, A. M., Okamoto, T. J., Ichimoto, K., Katsukawa, Y., Suematsu, Y., Tsuneta, S., Lites, B. W., Shimizu, T., 2008. Hinode sot observations of solar quiescent prominence dynamics. Astrophys. J. Lett. 676, L89–L92.

Berger, T. E., Slater, G., Hurlburt, N., Shine, R., Tarbell, T., Title, A., Lites, B. W., Okamoto, T. J., Ichimoto, K., Katsukawa, Y., Magara, T., Suematsu, Y., Shimizu, T., 2010. Quiescent prominence dynamics observed with the hinode solar optical telescope. i. turbulent upflow plumes. Astrophys. J. 716, 1288–1307.

Cao, W., Gorceix, N., Coulter, R., Wöger, F., Ahn, K., Shumko, S., Varsik, J., Coulter, A., Goode, P. R., 2010. Nasmyth focus instrumentation of the new solar telescope at big bear solar observatory. In: Society of Photo-Optical Instrumentation Engineers (SPIE) Conference Series. Vol. 7735 of Society of Photo-Optical Instrumentation Engineers (SPIE) Conference Series. p. 5.

Deng, H., Zhang, D., Wang, T., Ji, K., Wang, F., Liu, Z., Xiang, Y., Jin, Z., Cao, W., 2015. Objective image-quality assessment for high-resolution photospheric images by median filter-gradient similarity. Solar Phys. 290, 1479–1489.

Denker, C., 1998. Speckle masking imaging of sunspots and pores. Solar Phys. 180, 81–108.

Denker, C., Mascarinas, D., Xu, Y., Cao, W., Yang, G., Wang, H., Goode, P. R., Rimmele, T., 2005. High-spatial-resolution imaging combining high-order adaptive optics, frame selection, and speckle masking reconstruction. Solar Phys. 227, 217–230.

Feng, S., Deng, L., Shu, G., Wang, F., Deng, H., Ji, K., 2012. A subpixel registration algorithm for low psnr images. International Conference on Advanced Computational Intelligence, ICACI, 626–630.

Knox, K. T., Thompson, B. J., 1974. Recovery of images from atmospherically degraded short-exposure photographs. Astrophys. J. Lett. 193, L45–L48.

Korff, D., 1973. Analysis of a method for obtaining near-diffraction-limited information in the presence of atmospheric turbulence. Journal of the Optical Society of America 63, 971.

Labeyrie, A., 1970. Attainment of diffraction limited resolution in large telescopes by fourier analysing speckle patterns in star images. Astron. Astrophys. 6, 85.

Liu, G.-Q., Cheng, X.-M., Song, T.-F., Zhao, X.-J., 2011. The influence and control of wind loading on the one meter solar telescope servosystem. Opto-Electronic Engineering 39, 50–57.

Liu, Z., Xu, J., Gu, B.-Z., Wang, S., You, J.-Q., Shen, L.-X., Lu, R.-W., Jin, Z.-Y., et al., 2014. New vacuum solar telescope and observations with high resolution. Research in Astronomy and Astrophysics 14, 705–718.

Lohmann, A. W., Weigelt, G., Wirnitzer, B., 1983. Speckle masking in astronomy - triple correlation theory and applications. Applied Optics 22, 4028–4037.

Mikurda, K., von der Lühe, O., 2006. High resolution solar speckle imaging with the extended knox-thompson algorithm. Solar Phys. 235, 31–53.

Pehlemann, E., von der Lühe, O., 1989. Technical aspects of the speckle masking phase reconstruction algorithm. Astron. Astrophys. 216, 337–346.

Shen, Y., Liu, Y., Liu, Y. D., Chen, P. F., Su, J., Xu, Z., Liu, Z., 2015. Fine magnetic structure and origin of counter-streaming mass flows in a quiescent solar prominence. Astrophys. J. Lett. 814, L17.

Smithson, R. C., Tarbell, T. D., 1977. Correlation tracking study for meter-class solar telescope on space shuttle. Tech. rep.

Tandberg-Hanssen, E., 1995. Books-received - the nature of solar prominences. Science 269, 111.

Tyler, D. W., Suzuki, A. H., von Bokern, M. A., Keating, D. D., Roggemann, M. C., 1994. Optimal snr exposure time for speckle imaging: experimental results with frequency-dependent detector noise. In: Crawford, D. L., Craine, E. R. (Eds.), Instrumentation in Astronomy VIII. Vol. 2198 of Society of Photo-Optical Instrumentation Engineers (SPIE) Conference Series. pp. 1389–1397.

von der Lühe, O., 1983. A study of a correlation tracking method to improve imaging quality of ground-based solar telescopes. Astron. Astrophys. 119, 85–94.

von der Lühe, O., 1984. Estimating fried's parameter from a time series of an arbitrary resolved object imaged through atmospheric turbulence. Journal of the Optical Society of America A 1, 510–519.

von der Lühe, O., 1993. Speckle imaging of solar small scale structure. i - methods. Astron. Astrophys. 268, 374–390.

von der Lühe, O., 1994. Speckle imaging of solar small scale structure. 2: Study of small scale structure in active regions. Astron. Astrophys. 281, 889–910.

Weigelt, G., Wirnitzer, B., 1983. Image reconstruction by the speckle-masking method. Optics Letters 8, 389–391.

Weigelt, G. P., 1977. Modified astronomical speckle interferometry 'speckle masking'. Optics Communications 21, 55–59.

Yan, X.-L., Xue, Z.-K., Xiang, Y.-Y., Yang, L.-H., 2015. Fine-scale structures and material flows of quiescent filaments observed by the new vacuum solar telescope. Research in Astronomy and Astrophysics 15, 1725.

Yang, Y.-F., Qu, H.-X., Ji, K.-F., Feng, S., Deng, H., Lin, J.-B., Wang, F., 2015. Characterizing motion types of g-band bright points in the quiet sun. Research in Astronomy and Astrophysics 15, 569.